

Short Communication

In-situ Synthesis of Graphitic Carbon Nitride/Gold Nanoparticle Nanocomposites for Electrocatalytic Reduction of Iron(III)

Haitao Han¹, Dawei Pan^{1,*}, Mingyue Lin¹, Xueping Hu¹, Fei Li²

¹ Key Laboratory of Coastal Environmental Processes and Ecological Remediation, Yantai Institute of Coastal Zone Research (YIC), Chinese Academy of Sciences(CAS); Shandong Provincial Key Laboratory of Coastal Environmental Processes, YICCAS, Yantai Shandong 264003, P. R. China

² The Key Lab in Molecular and Nano-materials Probes of the Ministry of Education of China, College of Chemistry, Chemical Engineering and Materials Science, Shandong Normal University, Jinan Shandong 250014, P.R. China

*E-mail: dwpan@yic.ac.cn

Received: 14 August 2015 / Accepted: 5 September 2015 / Published: 30 September 2015

The graphitic carbon nitride/gold nanoparticle ($\text{g-C}_3\text{N}_4/\text{AuNP}$) nanocomposites were reported in this paper based on an in-situ synthetic method. After the protonation, ion-exchange, and chemical reduction processes, the $\text{g-C}_3\text{N}_4/\text{AuNP}$ nanocomposites were successfully obtained. The proposed nanocomposites were investigated by various optical and electrical techniques, including scanning electron microscopy (SEM), transmission electron microscopy (TEM), X-ray diffraction spectroscopy (XRD), X-ray photoelectron spectroscopy (XPS), cyclic voltammetry (CV), etc. The $\text{g-C}_3\text{N}_4/\text{AuNP}$ nanocomposites showed excellent electrochemical properties and their preliminary applications toward electrocatalytic reduction of ferric iron were investigated. These nanocomposites exhibit promising prospects for practical application in electrochemical analysis.

Keywords: Graphitic carbon nitride, gold nanoparticle, in-situ synthesis, nanocomposites, iron

1. INTRODUCTION

As the most stable allotrope of carbon nitride, graphitic carbon nitride ($\text{g-C}_3\text{N}_4$) has attracted a great deal of attention from experimental and theoretical communities, mainly because of its fascinating properties such as appropriate band gap, excellent biocompatibility, and good chemical stability [1-3]. Particularly, due to its special semiconductor (band gap of 2.7 eV) and visible light

absorption properties [4], g-C₃N₄ has already been widely used as non-metal catalysts for light degradation of organic dyes, photolysis of water to obtain hydrogen, and photocatalytic organic reactions [5-7]. Nowadays, lots of nanocomposites based on g-C₃N₄, such as carbon-doped g-C₃N₄ and Ti-doped g-C₃N₄, and so on, have been proposed to enhance the catalytic activity of g-C₃N₄ [8,9]. As a result, several of methods have been developed to fabricate g-C₃N₄ based nanocomposites [10,11].

On the other hand, gold nanoparticles (AuNPs) possess excellent properties, such as large surface-to-volume ratio, outstanding electrical properties, high surface reaction activity, strong adsorption ability, and excellent biocompatibility [12-15]. In a word, AuNPs possess excellent electrochemical properties and have been widely used as the decorator for nanomaterials.

In this paper, an in-situ method was employed as the effective strategy to synthesize the g-C₃N₄/AuNP nanocomposites. Firstly, g-C₃N₄ was protonated by hydrochloric acid (HCl) to form g-C₃N₄-H⁺Cl⁻. And then, Cl⁻ in g-C₃N₄-H⁺Cl⁻ was ion-exchanged by chloroaurate ions (AuCl₄⁻) which was in-situ reduced to AuNPs by chemical reductant subsequently. The properties of the proposed nanocomposites were studied by various optical and electrical methods, including X-ray diffraction spectroscopy (XRD), X-ray photoelectron spectroscopy (XPS), scanning electron microscopy (SEM), transmission electron microscopy (TEM), Fournier transformation infrared spectroscopy (FTIR), and cyclic voltammetry (CV). The preliminary application of g-C₃N₄/AuNP nanocomposites towards electrocatalytic reduction of Fe(III) was also investigated.

2. EXPERIMENTAL

2.1. Materials and apparatus

HAuCl₄ and melamine were supplied by Sinopharm Chemical Reagent Co., Ltd. Iron standard solution was purchased from Acros Organics (USA. <http://www.acros.com/>). All other chemicals are analytical reagents which used without further purification. The used deionized water (18.2 MΩ cm specific resistance) were obtained from Pall Cascada laboratory water system. The properties of the g-C₃N₄/AuNP nanocomposites were characterized by XRD (XRD-7000, Shimadzu Corporation), XPS (Kratos Amicus spectrometer), SEM (Hitachi S-4800), TEM (JEOL-1400), EDS (HORIBA EX-350), and FTIR (NicoletiS10). CHI 660E Electrochemical Work Station was used to carry out all the electrochemical experiments in which a conventional three-electrode cell was adopted. The g-C₃N₄/AuNP nanocomposites modified glassy carbon (GC) disk (3 mm in diameter) was used as the working electrode, with an Ag/AgCl electrode and platinum foil serving as the reference and counter electrodes, respectively.

2.2. Preparation of g-C₃N₄/AuNP nanocomposites

Firstly, g-C₃N₄ was synthesized through the condensation of melamine according to literature [1]. After, the synthesized g-C₃N₄ (0.5 g) was protonated by stirring with HCl (37%, 100 mL) for 3 hours at room temperature to form g-C₃N₄-H⁺Cl⁻. After filtered and thoroughly washed, g-C₃N₄-H⁺Cl⁻

was dispersed in 100 mL freshly deionized water once again with ultrasonication. Then, 2 mL HAuCl₄ (20 mmol L⁻¹) was added to the mixture with stirring, and the Cl⁻ was ion-exchanged by AuCl₄⁻. After removing of the not ion-exchanged HAuCl₄ (centrifugal and washing), excess NaBH₄ was added to the suspension drop to drop with stirring. The g-C₃N₄/AuNP nanocomposites were obtained after the suspension was centrifuged and washed sufficiently.

2.3. Fabrication of g-C₃N₄/AuNP nanocomposites modified electrode

The g-C₃N₄/AuNP nanocomposites modified GC (g-C₃N₄/AuNP/GC) electrode was prepared by dropping the g-C₃N₄/AuNP suspension (10 μL) on the surface of GC electrode and drying with an infrared lamp.

2.4. Electrochemical procedure

The g-C₃N₄/AuNP nanocomposites were electrochemically characterized by CV and differential pulse voltammetry (DPV). The CV experiments were carried out at a potential range of -0.2 to 1.5 V at a scan rate of 100 mV s⁻¹ in 10 ml 0.5 mol L⁻¹ H₂SO₄. The DPV responses of g-C₃N₄/AuNP/GC and bare GC electrodes to the electrocatalytic reduction Fe(III) with different concentrations (0, 10, and 20 μmol L⁻¹) were investigated in 0.1 mol L⁻¹ HCl solution with the scan range from 0.7 to 0.35 V.

3. RESULTS AND DISCUSSION

Protonation of g-C₃N₄ can provide the Cl⁻ for subsequent ion-exchange and improve its dispersion and ionic conductivity [3,16]. Various optical and electrical methods were used to study the properties of the resulting nanocomposites.

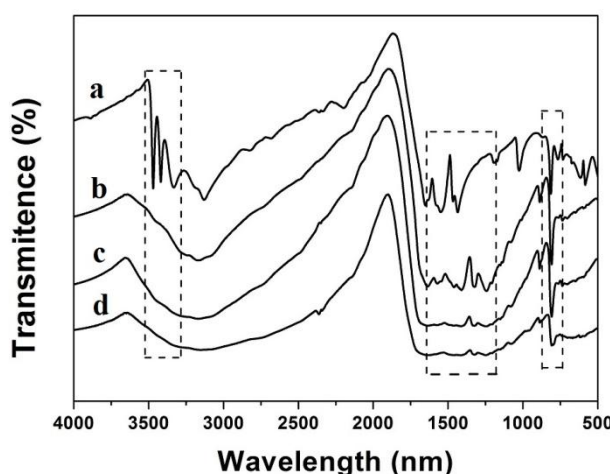


Figure 1. FTIR spectra of melamine (a), g-C₃N₄ (b), g-C₃N₄-H⁺Cl⁻ (c), and g-C₃N₄/AuNP nanocomposites (d).

3.1. FTIR spectrum of the g-C₃N₄/AuNP nanocomposites

FTIR spectroscopy was carried out to investigate whether this proposed synthesis process would damage the graphite-like structure of g-C₃N₄. Figure 1 shows the FTIR spectra of melamine (Figure 1a), g-C₃N₄ (Figure 1b), g-C₃N₄-H⁺Cl⁻ (Figure 1c), and g-C₃N₄/AuNP nanocomposites (Figure 1d). It can be concluded that after the condensation of melamine to g-C₃N₄, the bands of N-H (3300-3500 cm⁻¹) disappeared while the bands of C-N (1240-1643 cm⁻¹) and tri-s-triazine (810 cm⁻¹) retained. The FTIR spectra of g-C₃N₄-H⁺Cl⁻ and g-C₃N₄/AuNP nanocomposites is very similar to that of g-C₃N₄, which indicates that there is no damage to the graphite-like structure of g-C₃N₄ during the proposed in-situ synthesis process.

3.2. SEM images and EDS pattern of the g-C₃N₄/AuNP nanocomposites

To describe the morphology of the synthesized g-C₃N₄/AuNP nanocomposites, SEM images and EDS pattern were employed. Figure 2 illustrates the typical SEM photographs of g-C₃N₄ (Figure 2a), g-C₃N₄/AuNP nanocomposites (Figure 2b), and the EDS pattern of the g-C₃N₄/AuNP nanocomposites (Figure 2c). Obviously, g-C₃N₄ appears to have sheet structures in the SEM micrograph image, which is in accordance with the reported literature [17]. The morphology of the g-C₃N₄/AuNP nanocomposites is similar to that of g-C₃N₄, except for the uniformly distributed AuNPs on the g-C₃N₄ surface. The EDS pattern of the g-C₃N₄/AuNP nanocomposites indicates that C, N, Al, and Au are the major elements in the nanocomposites. C and N may come from g-C₃N₄, while Al may be attributed to the base aluminum foil. The presence of Au in the pattern confirms the existence of AuNPs on the g-C₃N₄ surface.

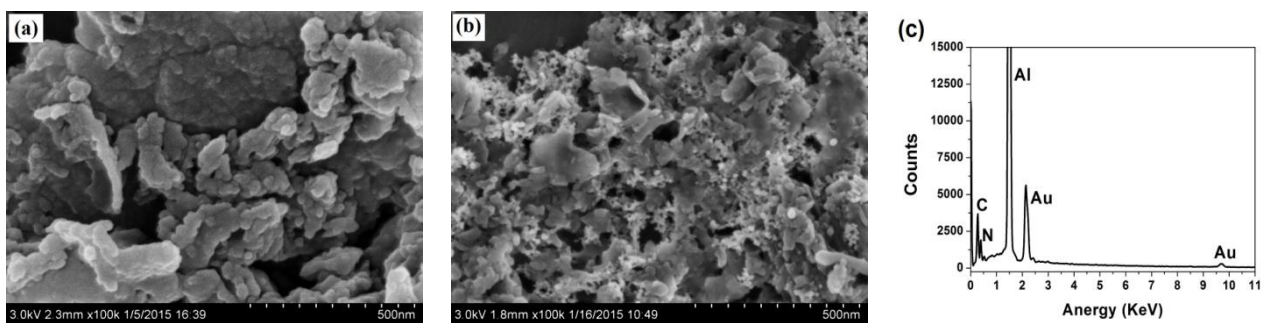


Figure 2. SEM images of g-C₃N₄ (a), g-C₃N₄/AuNP nanocomposites (b), and EDS pattern of g-C₃N₄/AuNP nanocomposites (c).

3.3. TEM images of the g-C₃N₄/AuNP nanocomposites

TEM images provide further evidence for the successful synthesis of the g-C₃N₄/AuNP nanocomposites. Figure 3 shows the TEM photographs of g-C₃N₄ (Figure 3a), and g-C₃N₄/AuNP nanocomposites (Figure 3b). It can be observed that g-C₃N₄ has sheet structures. As to the g-C₃N₄/AuNP nanocomposites, the morphology is clearly different from that of g-C₃N₄. The dispersion

of the sheet is more symmetrical and this may be caused by the cutting effect during the synthesis process. Furthermore, numerous uniform nanoparticles can be observed on the surface of g-C₃N₄/AuNP nanocomposites. In a word, almost 5 nm AuNPs were well distributed on the surface of g-C₃N₄.

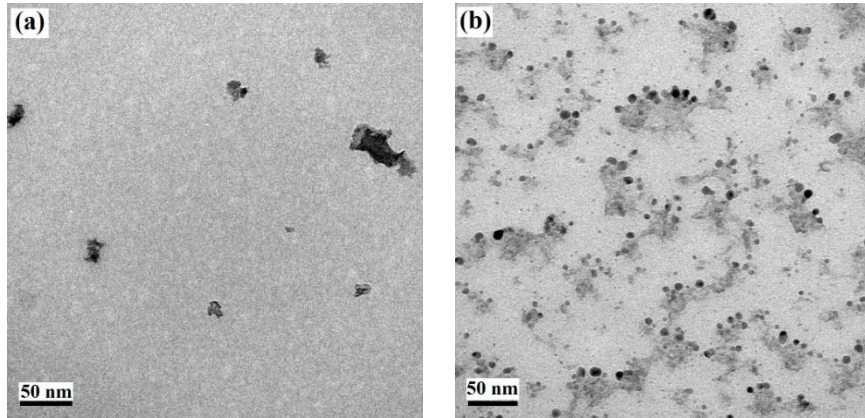


Figure 3. TEM images of g-C₃N₄ (a), and g-C₃N₄/AuNP nanocomposites (b)

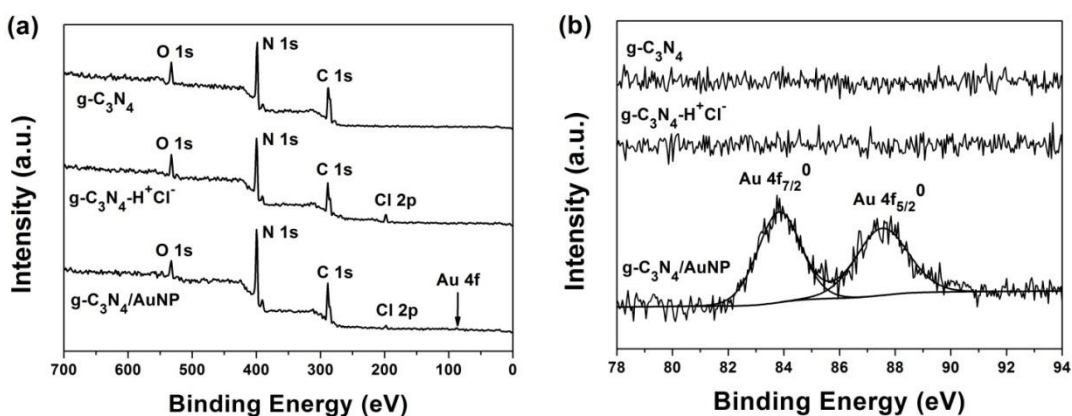


Figure 4. Survey (a) and Au 4f (b) XPS spectra of g-C₃N₄, g-C₃N₄-H⁺Cl⁻, and g-C₃N₄/AuNP nanocomposites.

3.4. XPS spectrum of the g-C₃N₄/AuNP nanocomposites

To further confirm the in-situ synthesis of the g-C₃N₄/AuNP nanocomposites, XPS was conducted. Figure 4 shows the survey (Figure 4a) and Au 4f (Figure 4b) XPS spectra of g-C₃N₄, g-C₃N₄-H⁺Cl⁻, and g-C₃N₄/AuNP nanocomposites. The appearance of Cl 2p in g-C₃N₄-H⁺Cl⁻ proves the successful protonation of g-C₃N₄. The Au 4f XPS spectrum of the g-C₃N₄/AuNP nanocomposites displays a doublet for Au⁰ due to Au 4f_{7/2} and Au 4f_{5/2} spin-orbit coupling, which proves the presence of AuNPs. The decrease of Cl 2p peak in g-C₃N₄/AuNP nanocomposites may be caused by the ion-exchange between Cl⁻ and AuCl₄⁻, which proves that in-situ growth of AuNPs. Moreover, the C/N ratios of g-C₃N₄, g-C₃N₄-H⁺Cl⁻, and g-C₃N₄/AuNP nanocomposites are (56/44, 51/45, and 52/46

respectively) very close, which indicates that the component and graphite-like structure of g-C₃N₄ were not damaged during the proposed in-situ synthesis process.

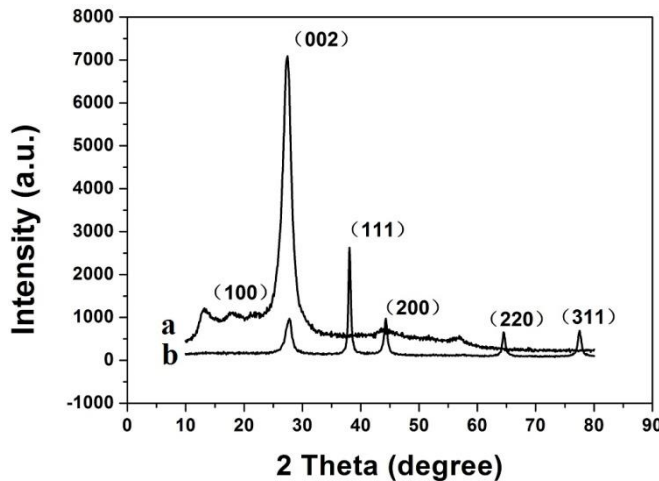


Figure 5. XRD patterns of g-C₃N₄ (a) and g-C₃N₄/AuNP nanocomposites (b).

3.5. XRD pattern of the g-C₃N₄/AuNP nanocomposites

XRD is a powerful and effective method for investigating the crystalline properties of the as-synthesized nanomaterials. Figure 5 shows the XRD patterns of g-C₃N₄ (Figure 5a), and g-C₃N₄/AuNP nanocomposites (Figure 5b). In Figure 5a, a typical g-C₃N₄ structure is suggested by two obvious peaks. The strongest peak at $2\theta = 27.48^\circ$ is a characteristic interlayer stacking peak of aromatic systems, and can be indexed as the (002) plane for graphitic materials [1]. The calculated interplanar distance of aromatic units is $d = 0.324$ nm. The relatively weak peak at $2\theta = 13.52^\circ$ indexed as (100) plane can be associated with an in-plane structural packing motif. As to the g-C₃N₄/AuNP nanocomposites, the typical diffraction peaks at $2\theta = 38.11^\circ$, 44.29° , 64.51° and 77.51° corresponding to the (111), (200), (220), and (311) lattice planes of the gold face-centered cubic crystal appear attractively except for the (002) characteristic peak of g-C₃N₄ [18,19].

From all the results discussed above, it can be concluded that the g-C₃N₄/AuNP nanocomposites were synthesized successfully through the in-situ strategy and the graphite-like structure of g-C₃N₄ was retained during the synthesis process.

3.6. Electrochemical behaviors and potential application of the g-C₃N₄/AuNP nanocomposites

To investigate the electrochemical properties of the target g-C₃N₄/AuNP nanocomposites, CV curves of the bare GC, and g-C₃N₄/AuNP/GC electrodes in 0.5 mol L⁻¹ H₂SO₄ solution from 0.2 to 1.5 V with a scan rate of 100 mV s⁻¹ are presented in Figure 6. It can be observed that there is no redox peak obtained for the bare GC electrode (Figure 6a). However, a sharp reduction peak and an oxidation peak can be seen from the g-C₃N₄/AuNP/GC electrode (Figure 6b). Obviously, the peaks were caused by the redox of AuNPs. Moreover, AuNPs can facilitate electron transfer to improve the electroconductivity of the synthesized nanomaterials.

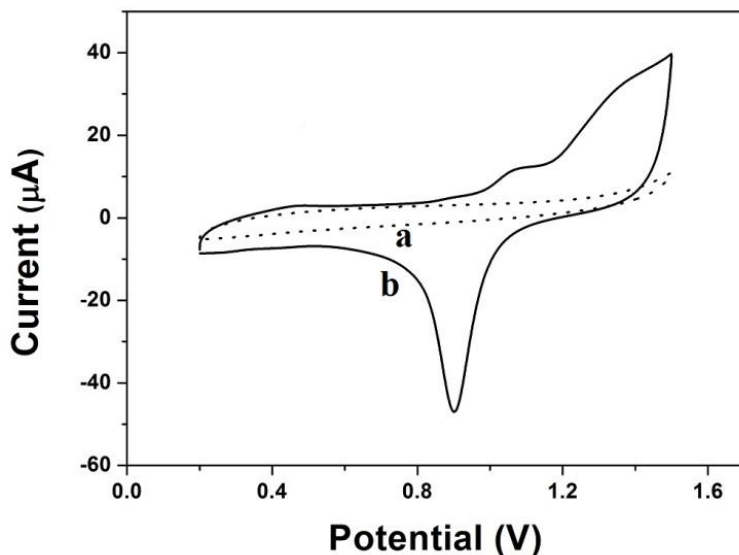


Figure 6. Cyclic voltammograms of bare GC (a) and $\text{g-C}_3\text{N}_4/\text{AuNP}/\text{GC}$ (b) electrodes in 0.5 mol L^{-1} H_2SO_4 solution.

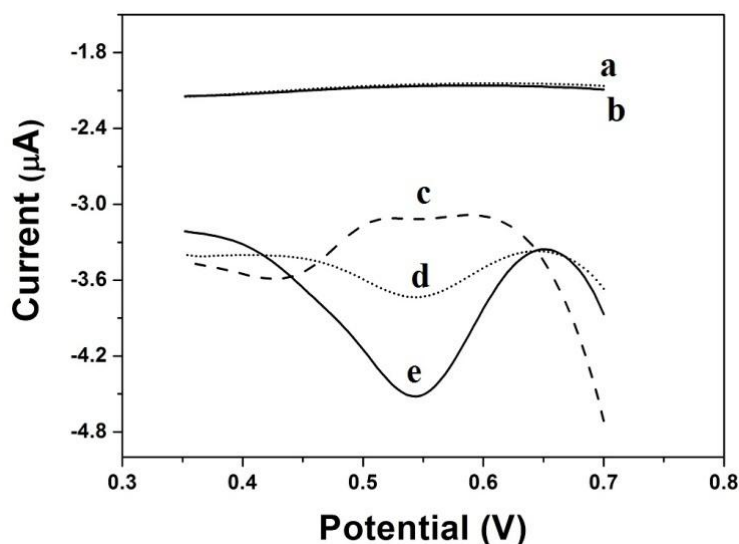


Figure 7. Differential pulse voltammograms of bare GC electrode without (a) and with (b) $10 \mu\text{mol L}^{-1}$ Fe(III), $\text{g-C}_3\text{N}_4/\text{AuNP}/\text{GC}$ electrode without (c), with $10 \mu\text{mol L}^{-1}$ (b) and $20 \mu\text{mol L}^{-1}$ (e) Fe(III) in 0.1 mol L^{-1} HCl.

Figure 7 shows the differential pulse voltammetry (DPV) responses toward Fe(III) reduction at two different electrodes in 0.1 mol L^{-1} HCl. There is no reduction peak at the bare GC electrode without and with $10 \mu\text{mol L}^{-1}$ Fe(III) (Figure 7a, b). In other words, it is not possible to detect $10 \mu\text{mol L}^{-1}$ Fe(III) using the unmodified GC electrode. However, at the $\text{g-C}_3\text{N}_4/\text{AuNP}/\text{GC}$ electrode, contrast to the DPV response without Fe(III) (Figure 7c), a sharp reduction peak at about 0.54 V was observed when $10 \mu\text{mol L}^{-1}$ (Figure 7d) and $20 \mu\text{mol L}^{-1}$ (Figure 7e) Fe(III) was added. Distinctly, the reduction peak was due to the reduction of Fe(III) and this shows the excellent electrocatalytic activity of the g-

$\text{C}_3\text{N}_4/\text{AuNP}$ nanocomposites towards the reduction of Fe(III). This makes it feasible to determinate the Fe(III) concentration with the modified electrode. Additionally, it should be noted that the reduction peak potential is almost at 0.54 V, which means that the nanocomposites modified electrode has much higher onset reduction potential than most of the electrodes in the electrocatalytical reduction of Fe(III) [20,21]. And this also shows the high electrocatalytic activity of the proposed nanocomposites. The excellent electrochemical properties of the $\text{g-C}_3\text{N}_4/\text{AuNP}$ nanocomposites exhibit a promising prospect for the electrochemical detection of iron.

4. CONCLUSIONS

An in-situ method based on ion-exchange was reported here to successfully synthesize the $\text{g-C}_3\text{N}_4/\text{AuNP}$ nanocomposites. The $\text{g-C}_3\text{N}_4$ was protonated by HCl and ion-exchanged by AuCl_4^- and then reduced to the target nanocomposites in-situ. Extensive characterizations of the $\text{g-C}_3\text{N}_4/\text{AuNP}$ nanocomposites were studied and the results showed that AuNPs were well distributed on the surface of the $\text{g-C}_3\text{N}_4$. Additionally, the nanocomposites have good electrocatalytic responses to Fe(III) reduction and can be used for development of iron sensors.

ACKNOWLEDGEMENTS

This work was financially supported by the National Natural Science Foundation of China (41276093), the Youth Innovation Promotion Association (2011170) and the Outstanding Young Scientists Program of CAS.

References

1. H. H. Ji, F. Chang, X. F. Hu, W. Qin, and J. W. Shen, *Chem. Eng. J.*, 218, 183 (2013).
2. L. Ge, C.C. Han, J. Liu, and Y.F. Li, *Appl. Catal. A-Gen.*, 409 (2011) 215.
3. L.C. Chen, D.J. Huang, S.Y. Ren, T.Q. Dong, Y.W. Chi, and G.N. Chen, *Nanoscale*, 5 (2013) 225.
4. L.M. Song, S.J. Zhang, X.Q. Wu, H.F. Tian, and Q.W. Wei, *Ind. Eng. Chem. Res.*, 51 (2012) 9510.
5. C.O. Song, W.H. Shin, H.S. Choi, and J.K. Kang, *J. Mater. Chem.*, 20 (2010) 7276.
6. L.M. Song, S.J. Zhang, X.Q. Wu, and Q.W. Wei, *Chem. Eng. J.*, 184 (2012) 256.
7. X.H. Li, J.S. Chen, X.H. Wang, J.H. Sun, and A. Markus, *J. Am. Chem. Soc.*, 133 (2011) 8074.
8. Y.P. Li, S.L. Wu, L.Y. Huang, J.L. Wang, H. Xu, and H.M. Li, *Mater. Lett.*, 137 (2014) 281.
9. Y.G. Wang, Y.Z. Wang, Y.T. Chen, C.C. Yin, Y.H. Zuo, and L.F. Cui, *Mater. Lett.*, 139 (2015) 70.
10. Y.T. Gong, P.F. Zhang, X. Xu, Y. Li, H.R. Li, and Y. Wang, *J. Catal.*, 297 (2013) 272.
11. Y.M. He, J. Cai, T.T. Li, Y. Wu, H.J. Lin, L.H. Zhao, and M.F. Luo, *Chem. Eng. J.*, 215 (2013) 721.
12. Z. Zhang, H. Chen, C. Xing, M. Guo, F. Xu, X. Wang, H. Gruber, B. Zhang, and J. Tang, *Nano Res.*, 4 (2011) 599.
13. S. Li, Y. Shi, L. Liu, L. Song, H. Pang, and J. Du, *Electrochim. Acta*, 85 (2012) 628.
14. C. Basavaraja, W.J. Kim, P.X. Thinh, and D.S. Huh, *Mater. Lett.*, 77 (2012) 41.
15. H.E. Lee, Y.O. Kang, and S.H. Choi, *Int. J. Electrochem. Sci.*, 9 (2014) 6793.
16. Y.J. Zhang, A. Thomas, M. Antonietti, and X.C. Wang, *J. Am. Chem. Soc.*, 131 (2009) 50.
17. N. Tian, H. W. Huang, Y. He, Y. X. Guo, and Y. H. Zhang, *Colloids Surf. A*, 467 (2015) 188.

18. Z. Wang, K. Shang, J. Dong, Z. Cheng, and S. Ai, *Microchim. Acta*, 179 (2012) 227.
19. Y. Liu, L. Liu, M. Yuan, and R. Guo, *Colloids Surf. A*, 417 (2013) 18.
20. R.K. Shervedani, A. Hatefi-Mehrjardi, and A. Asadi-Farsani, *Anal. Chim. Acta*, 601 (2007) 164.
21. M.Y. Lin, H.T. Han, D.W. Pan, H.Y. Zhang, and Z.C. Su, *Microchim. Acta*, 182 (2015) 805.

© 2015 The Authors. Published by ESG (www.electrochemsci.org). This article is an open access article distributed under the terms and conditions of the Creative Commons Attribution license (<http://creativecommons.org/licenses/by/4.0/>).